JACS
JOURNAL OF THE AMERICAN CHEMICAL SOCIETY

Communication

pubs.acs.org/JACS

Driving the Oxygen Evolution Reaction by Nonlinear Cooperativity in Bimetallic Coordination Catalysts

Benjamin Wurster,[†] Doris Grumelli,*[,‡] Diana Hötger,[†] Rico Gutzler,[†] and Klaus Kern[†,§]

[†]Max Planck Institute for Solid State Research, Heisenbergstrasse 1, 70569 Stuttgart, Germany

[‡]Instituto de Investigaciones Fisicoquímicas Teóricas y Aplicadas (INIFTA), Facultad de Ciencias Exactas, Universidad Nacional de La Plata, CONICET, Sucursal 4 Casilla de Correo 16, 1900 La Plata, Argentina

[§]Ecole Polytechnique Fédérale de Lausanne, 1015 Lausanne, Switzerland

Supporting Information

ABSTRACT: Developing efficient catalysts for electrolysis, in particular for the oxygen evolution in the anodic half cell reaction, is an important challenge in energy conversion technologies. By taking inspiration from the catalytic properties of single-atom catalysts and metalloproteins, we exploit the potential of metal−organic networks as electrocatalysts in the oxygen evolution reaction (OER). A dramatic enhancement of the catalytic activity toward the production of oxygen by nearly 2 orders of magnitude is demonstrated for novel heterobimetallic organic catalysts compared to metallo-porphyrins. Using a supramolecular approach we deliberately place single iron and cobalt atoms in either of two different coordination environments and observe a highly nonlinear increase in the catalytic activity depending on the coordination spheres of Fe and Co. Catalysis sets in at about 300 mV overpotential with high turnover frequencies that outperform other metal−organic catalysts like the prototypical hangman porphyrins.

Electrochemical splitting of water into H_2 and O_2 provides a source of clean and renewable energy.[1,2] The dominant limitation in water electrolysis ($4OH^- \rightarrow O_2 + 2H_2O + 4e^-$ in alkaline electrolytes) is the large overpotential necessary for driving the oxygen evolution reaction (OER), in which four electrons are transferred and a covalent O−O bond is formed. This is achieved by using a catalyst to overcome kinetic barriers and to expedite the reaction.[3] In particular single-atom catalyst have attracted considerable attention for the optimization of activity, selectivity, and stability of heterogeneous catalysts.[4] Furthermore, bimetallic catalysts have been shown to be highly selective in asymmetric chemical transformations[5] and to increase the catalytic activity in chemical reactions.[6−9] A prominent class of bimetallic materials that function as catalysts for various reactions are metalloenzymes,[10] in which redox active ions are connected by bridging organic ligands.

Other examples are diverse and include metal−organic catalysts such as porphyrins,[11,12] core/shell metal nanoparticles,[13] and well-defined bimetallic surfaces. Oxygen evolution in nature is carried out by photosystem II on a multimetallic Mn_4CaO_5 cluster, which produces O_2 at high turnover frequencies of 100−400 s^{-1},[14] values that only recently have been achieved by artificial metal−organic water-oxidation catalysts.[15,16]

We focus on surface supported metal−organic structures[17] and their suitability as electrocatalysts for the OER.[18,19] Two-dimensional metal−organic networks have previously been reported as electrocatalytically active materials for the oxygen reduction reaction[19] in an experimental approach, which is here extended to bimetallic networks of *meso*-substituted porphyrins.[20−22] The advantage of using porphyrins to create a bimetallic structures rests on their ability to host a wide range of metals within the macrocycle[23,24] and to coordinate a second metal through its substituents. So far, 2D homometallic porphyrin networks have been synthesized almost exclusively including only one type of metal,[22] with few notable exceptions.[25] More specifically, free-base porphyrins substituted at their *meso*-positions with pyridyl groups have been studied by electrochemical-scanning tunneling microscopy[26,27] and can be used to template metal centers on surfaces.[28]

We report how the production of oxygen from water using homo- and heterobimetallic catalysts can be boosted by a suitable insertion of metal centers in an organic environment. A home-built transfer system between ultrahigh vacuum (UHV) and EC cell within a controlled argon atmosphere was used for sample transfer, inhibiting the oxidation of the sample prior to EC and thus ensuring perfect cleanliness.[19] The catalyst are prepared as monolayers in UHV on clean Au(111) surfaces and imaged by scanning tunneling microscopy (STM). The metallo-porphyrins 5,10,15,20-tetra(4-pyridyl)-21*H*,23*H*-porphyrine (H_2TPyP), 5,10,15,20-tetra(4-pyridyl)21*H*,23*H*-porphyrine iron(III) chloride (FeTPyP) and 5,10,15,20-tetra(4-pyridyl)21*H*,23*H*-porphyrine cobalt(III) chloride (CoTPyP) were purchased from Frontier Scientific. Oxygen evolution reaction (OER) was carried out in a 0.1 M NaOH solution (see Supporting Information for additional details). X-ray photoelectron spectroscopy (XPS) was used to clarify the oxidation number of the metal centers and to confirm the stability of the catalyst.

Figure 1a shows the chemical structure of the metal pyridyl−porphyrin (M^1TPyP) and schematizes how the incorporation of the second metal center (M^2) creates bimetallic structures (M^1TPyP-M^2, M^1, M^2 = Fe, Co). Figure 1b shows an STM image of a monolayer of the CoTPyP-Co catalyst on Au(111)

Received: October 7, 2015
Published: March 3, 2016

DOI: 10.1021/jacs.5b10484
J. Am. Chem. Soc. 2016, 138, 3623−3626

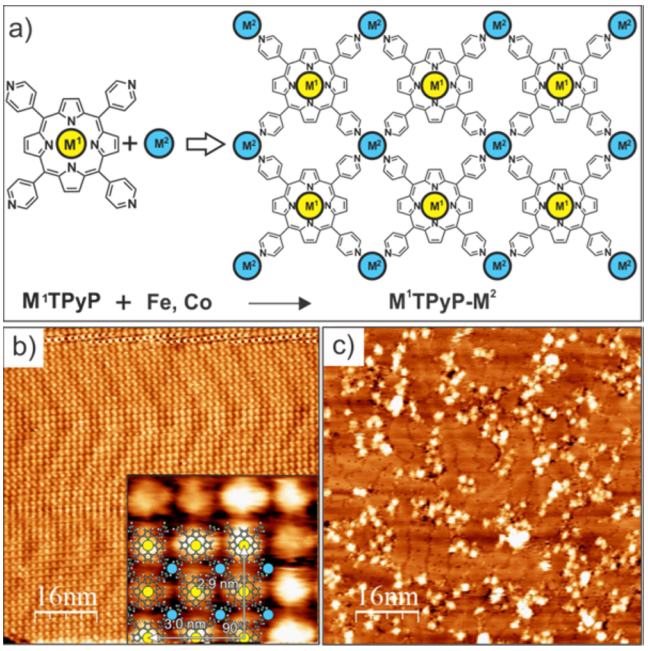

Figure 1. (a) Chemical structure of metal-5,10,15,20-tetra(4-pyridyl)-21*H*,23*H*-porphyrine M^1-TPyP where M^1 = Fe or Co, and model of the extended bimetallic catalyst. STM topographs of (b) monolayer of the freshly prepared CoTPyP-Co catalyst on Au(111) (V_{bias} = −1.1 V, I_{tunnel} = 0.2). Inset: molecular resolution image with model and lattice vectors superimposed (CoTPyP-Fe). Color legend: Fe (cyan), Co (yellow), C (gray), N (green), H (white). (c) CoTPyP-Co active catalyst after OER (V_{bias} = 0.8 V, I_{tunnel} = 0.2 nA).

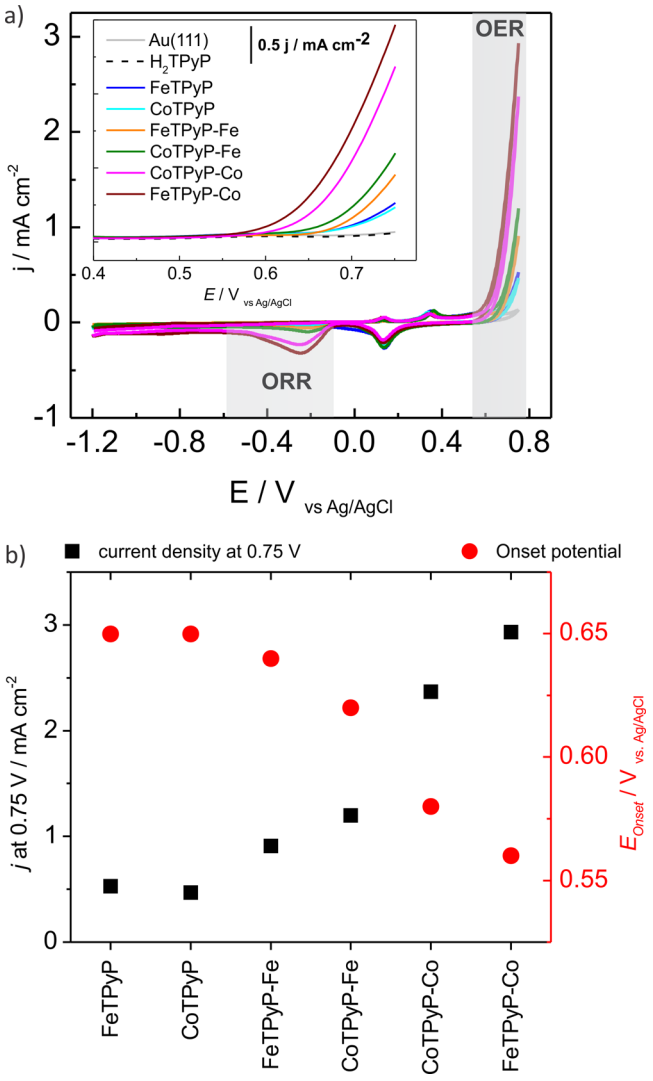

Figure 2. (a) Cyclic voltammetry at 0.05 V s^{-1} in NaOH 0.1 M Ar saturated solution for all molecular catalysts. Inset: anodic branch of cyclic voltammetry for H_2TPyP (black dotted line) and bare Au(111) electrode (gray) CoTPyP (light blue), FeTPyP (blue), FeTPyP-Fe (orange), CoTPyP-Fe (green), CoTPyP-Co (pink), and FeTPyP-Co (wine). (b) Current density at 0.75 V (black squares) and onset potentials (red circles) extracted from panel a.

immediately after preparation in UHV. A bright protrusion within the macrocycle is attributed to the central metal atom M^1. The second metal is coordinated by four pyridyl groups between the molecules, which leads to a rectangular arrangement of the molecular rows (see inset in Figure 1b). For more details of the molecular preparation and arrangement of the freshly prepared catalyst see Figure SI-1. All bimetallic catalysts with different metal combinations show the same topography, indicating a negligible influence of the type of metal on the structure of the coordination networks (Figure SI-2). XPS evidence that Co and Fe are in the +2 oxidation state in both coordination environments (Figure SI-3), demonstrating that the evaporated metal M^2 is coordinated to organic ligands and excluding the possibility of metal cluster formation. Figure 1c shows an STM image of the CoTPyP-Co catalytically active structure on Au(111) after EC. The square grid structure is not preserved and new features (high contrast in the STM image indicating large vertical height) are observable after OER, which likely are the catalytically active structures that persist on the surface. XPS performed after electrocatalysis (Figure SI-3) confirms that both metal centers remain in the +2 oxidation state and that the chemical structures remain intact.

Figure 2 shows the catalytic activities toward OER of all catalyst. As expected, no catalytic activity is observed for bare Au(111) (Figure 2a gray line, see inset) and H_2TPyP monolayer (dashed line). A detailed attribution of redox signals in the CV is given in Figure SI-4. Both single-metal porphyrins FeTPyP and CoTPyP (blue and cyan, respectively) show an increase in the current density as a measure of the catalytic activity above 0.65 V associated with the evolution of oxygen.[29]

The polarization curves of FeTPyP-Fe and CoTPyP-Fe (orange and green, respectively) are shifted to lower overpotentials (faster reaction kinetics), and a steeper slope leads to a higher current density at 0.75 V compared to FeTPyP and CoTPyP. Taking advantage of the versatility of our fabrication method, we prepared the same bimetallic catalyst with Co as second metal. The onset potentials extracted from the polarization curves of FeTPyP-Co (wine) and CoTPyP-Co (pink) are likewise shifted to lower overpotentials and increased current densities are observed. For a clearer comparison of the catalytic activities, the current density at 0.75 V and the onset potential of the different samples extracted from Figure 2a are presented in Figure 2b (see Figure SI-5 for reproducibility on different samples). The current densities are much larger than in previously reported OER on metallo-porphyrins prepared by conventional solution methods[29] and comparable to those achieved using hangman porphyrins.[30] The hangman-porphyrin catalyst, however, exhibits a much larger number of catalytically active sites per geometric area and thus a lower efficiency per atom compared to the M^1TPyP-M^2 layers. The thermodynamic

DOI: 10.1021/jacs.5b10484
J. Am. Chem. Soc. 2016, 138, 3623−3626

potential for water oxidation in our experimental conditions (pH = 13) lies at 0.25 V vs Ag/AgCl, only 300 mV lower than the onset potential of FeTPyP-Co. This low overpotential compares favorably to hangman porphyrins (overpotential of ~600 mV)[30] and Cu-based water oxidation catalysts (above 500 mV).[31]

Direct evidence that water splitting takes place is the presence of a cathodic peak in the cyclic voltammetry curves shown in Figure 2a. The peak located at −0.3 V corresponds to the reduction of O_2, which originates from the previous OER during the anodic scan. No O_2 is present in solution prior to OER in the Ar saturated solution. The area of the peak at −0.3 V for each network is thus a direct measure of the O_2 produced during OER. The values are in perfect agreement with the catalytic activity presented in Figure 2 following the sequence of increasing catalytic activity: M^1TPyP < M^1TPyP-Fe < M^1TPyP-Co. A complete list of O_2 produced during OER and the turnover frequencies (TOF, see SI for details on calculation) is given in Table 1. The TOFs are remarkably large even for the metallo-

Table 1. Amount of O_2 (produce during OER) Detected in the Cathodic Scan (ORR) and TOF for Each Network; See Supporting Information for Details

network	O_2 (nmol/cm^2) reduced in ORR	TOF (s^{-1})
FeTPyP	0.13	1.7
CoTPyP	0.16	2.2
FeTPyP-Fe	0.50	3.1
CoTPyP-Fe	0.71	3.7
CoTPyP-Co	2.69	10.7
FeTPyP-Co	3.43	12.2

porphyrins, and the bimetallic catalysts exhibit high rates superior to other metal−organic catalysts. For instance, the hangman porphyrin has a reported TOF of 0.81 s^{-1},[30] and 1.3 s^{-1} can be achieved with an iron complex.[32] M^1TPyP-M^2 catalysts are stable and show little degradation over time in the course of 15 polarization curves (Figure SI-6).

XPS and STM experiments were performed after OER electrochemical experiments to study the stability of the bimetallic catalyst. XPS (Figure SI-3) confirms the chemical integrity of the catalyst after EC, no major chemical shifts are observed for any of the elements and in particular Fe and Co remain in the +2 oxidation state. In Figure 3 are depicted the Co 2p core-level spectra compared for CoTPyP-Co in the freshly prepared catalyst (red), the catalyst after OER (wine) and with Co on bare Au(111) (yellow). The Co $2p_{3/2}$ peak in the catalyst before and after OER lies at ~780.2 eV, the value expected for Co(II).[33−35] Co in absence of organic ligands is metallic with its peak at ~778.7 eV. This observation confirms the stability of the catalyst in which the coordination environment of the metals remains unchanged during EC and the persistence of the +2 oxidation number relevant for OER.

For the catalyst in absence of a second metal, the better catalytic activity of CoTPyP with respect to FeTPyP is in agreement with literature[29,36] and has its origin in the strong interaction of the Co centers with the oxygen of the hydroxide ions.[29] Adding Fe as secondary metal to FeTPyP and CoTPyP increases the amount of generated O_2 by a factor of 14 and 4, respectively. Adding Co to both networks increases O_2 generation by factors of 86 and 20. The number of catalytically active sites, assuming each metal atom on the surface contributes as redox center, increases only 2-fold after addition of the second metal. The increased catalytic activity is thus not merely a

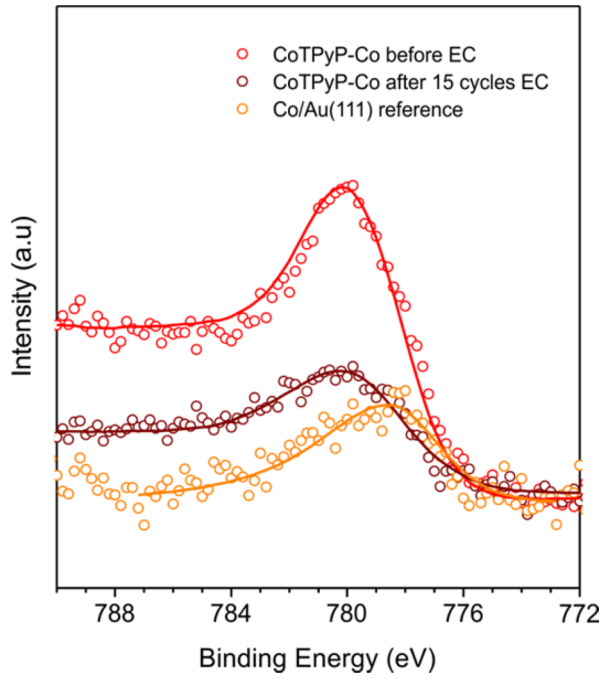

Figure 3. Co XPS data of freshly prepared CoTPyP-Co network (red), CoTPyP-Co after OER (wine), and Co evaporated on Au(111) as a control experiment (yellow).

consequence of the increased number of catalytic centers, but stems from more fundamental properties such as changes in the electronic structure of the metals in mono- vs bimetallic catalysts as a result of synergetic effects of the two metal centers.[7,8] The presumably large spatial separation between two metal centers in the M^1TPyP-M^2 catalysts precludes the direct cooperative interplay of two centers in the redox process of one substrate molecule, yet the addition of M^2 significantly enhances the activity of M^1TPyP. The catalysts in which Co is coordinated by the pyridine groups of M^1TPyP outperform the catalysts with Fe as secondary metal atom. However, FeTPyP-Co is a better catalyst than CoTPyP-Co, while CoTPyP-Fe outperforms FeTPyP-Fe. This strong asymmetry highlights the importance of the coordination environment of the metal center and suggests the pyridyl-Co moiety as the critical site for OER. A synergetic effect of two proximate metal ions is widely observed in both biological and synthetic bimetallic systems.[6] The extended π-electron system of the porphyrin macrocycle might be able to promote weak coupling of the two metal centers, and the surface *trans* effect (charge donation from/to surface) will influence the electronic structure of the metal centers and their ability to stabilize different reaction intermediates.[37] Preliminary X-ray absorption spectroscopy suggest coupling between Fe and Co in the FeTPyP-Co network, whose origin might be the same as the underlying reason for the network's increased catalytic activity. Additional DFT calculation, of course, can also help to elucidate the details of the reaction and will be evoked to assemble a concise picture of the processes at play.

In summary, we have engineered heterobimetallic catalysts that show a nonlinear increased catalytic activity toward the evolution of oxygen compared to homometallic catalysts. Compared to metallo-porphyrins the catalytic activity can be increased by almost 2 orders of magnitude in heterometallic catalysts. Overall, we report outstanding overpotentials and turnover frequencies of bimetallic catalysts compared to various

DOI: 10.1021/jacs.5b10484
J. Am. Chem. Soc. 2016, 138, 3623−3626

other metal−organic water oxidation catalysts. The combinatorial approach allows the positioning of different metal centers within the network in coordination environments that result in Co(II) and Fe(II) metal species, which decisively influences the catalytic properties of these materials. This dual distribution of single-atom catalytic centers offers the possibility to control the interplay of different metal centers. First, the porphyrin core macrocycle can host a wide range of metals. Second, porphyrins with a wide variety of *meso*-substituents are available for the coordination of the second metal center by different ligands. These two parameters span a broad combinatorial set providing a large number of unique bi- and mulitmetallic catalytic materials that can be used to further improve their catalytic properties.

■ ASSOCIATED CONTENT

Supporting Information

The Supporting Information is available free of charge on the ACS Publications website at DOI: 10.1021/jacs.5b10484.

Additional STM, XPS, and EC data and details on data analysis (PDF)

■ AUTHOR INFORMATION

Corresponding Author

*doris@inifta.unlp.edu.ar

Notes

The authors declare no competing financial interest.

■ ACKNOWLEDGMENTS

This work was supported by the Baden-Württemberg Stiftung.

■ REFERENCES

(1) Cao, R.; Lai, W.; Du, P. *Energy Environ. Sci.* **2012**, *5*, 8134−8157.
(2) Walter, M. G.; Warren, E. L.; McKone, J. R.; Boettcher, S. W.; Mi, Q.; Santori, E. A.; Lewis, N. S. *Chem. Rev.* **2010**, *110*, 6446−6473.
(3) Koper, M. T. M. *J. Electroanal. Chem.* **2011**, *660*, 254−260.
(4) Yang, X.-F.; Wang, A.; Qiao, B.; Li, J.; Liu, J.; Zhang, T. *Acc. Chem. Res.* **2013**, *46*, 1740−1748.
(5) Park, J.; Hong, S. *Chem. Soc. Rev.* **2012**, *41*, 6931−6943.
(6) Bosnich, B. *Inorg. Chem.* **1999**, *38*, 2554−2562.
(7) Steinhagen, H.; Helmchen, G. *Angew. Chem., Int. Ed. Engl.* **1996**, *35*, 2339−2342.
(8) van den Beuken, E. K.; Feringa, B. L. *Tetrahedron* **1998**, *54*, 12985−13011.
(9) van der Vlugt, J. I. *Eur. J. Inorg. Chem.* **2012**, *2012*, 363−375.
(10) Prabhulkar, S.; Tian, H.; Wang, X.; Zhu, J.-J.; Li, C.-Z. *Antioxid. Redox Signaling* **2012**, *17*, 1796−1822.
(11) Blusch, L. K.; Mitevski, O.; Martin-Diaconescu, V.; Pröpper, K.; DeBeer, S.; Dechert, S.; Meyer, F. *Inorg. Chem.* **2014**, *53*, 7876−7885.
(12) Fuerte, A.; Corma, A.; Iglesias, M.; Morales, E.; Sánchez, F. *Catal. Lett.* **2005**, *101*, 99−103.
(13) Porter, N. S.; Wu, H.; Quan, Z.; Fang, J. *Acc. Chem. Res.* **2013**, *46*, 1867−1877.
(14) Dismukes, G. C.; Brimblecombe, R.; Felton, G. A. N.; Pryadun, R. S.; Sheats, J. E.; Spiccia, L.; Swiegers, G. F. *Acc. Chem. Res.* **2009**, *42*, 1935−1943.
(15) Barnett, S. M.; Goldberg, K. I.; Mayer, J. M. *Nat. Chem.* **2012**, *4*, 498−502.
(16) Duan, L.; Bozoglian, F.; Mandal, S.; Stewart, B.; Privalov, T.; Llobet, A.; Sun, L. *Nat. Chem.* **2012**, *4*, 418−423.
(17) Barth, J. V.; Costantini, G.; Kern, K. *Nature* **2005**, *437*, 671−679.
(18) Fabris, S.; Stepanow, S.; Lin, N.; Gambardella, P.; Dmitriev, A.; Honolka, J.; Baroni, S.; Kern, K. *Nano Lett.* **2011**, *11*, 5414−5420.
(19) Grumelli, D.; Wurster, B.; Stepanow, S.; Kern, K. *Nat. Commun.* **2013**, *4*, 2904.
(20) Auwärter, W.; Weber-Bargioni, A.; Brink, S.; Riemann, A.; Schiffrin, A.; Ruben, M.; Barth, J. V. *ChemPhysChem* **2007**, *8*, 250−254.
(21) Auwärter, W.; Weber-Bargioni, A.; Riemann, A.; Schiffrin, A.; Gröning, O.; Fasel, R.; Barth, J. V. *J. Chem. Phys.* **2006**, *124*, 194708.
(22) Li, Y.; Xiao, J.; Shubina, T. E.; Chen, M.; Shi, Z.; Schmid, M.; Steinrück, H.-P.; Gottfried, J. M.; Lin, N. *J. Am. Chem. Soc.* **2012**, *134*, 6401−6408.
(23) Auwärter, W.; Écija, D.; Klappenberger, F.; Barth, J. V. *Nat. Chem.* **2015**, *7*, 105−120.
(24) Gottfried, J. M. *Surf. Sci. Rep.* **2015**, *70*, 259−379.
(25) El Garah, M.; Marets, N.; Mauro, M.; Aliprandi, A.; Bonacchi, S.; De Cola, L.; Ciesielski, A.; Bulach, V.; Hosseini, M. W.; Samorì, P. *J. Am. Chem. Soc.* **2015**, *137*, 8450−8459.
(26) Ye, T.; He, Y.; Borguet, E. *J. Phys. Chem. B* **2006**, *110*, 6141−6147.
(27) He, Y.; Ye, T.; Borguet, E. *J. Am. Chem. Soc.* **2002**, *124*, 11964−11970.
(28) Lin, T.; Kuang, G.; Wang, W.; Lin, N. *ACS Nano* **2014**, *8*, 8310−8316.
(29) De Wael, K.; Adriaens, A. *Talanta* **2008**, *74*, 1562−1567.
(30) Dogutan, D. K.; McGuire, R.; Nocera, D. G. *J. Am. Chem. Soc.* **2011**, *133*, 9178−9180.
(31) Zhang, T.; Wang, C.; Liu, S.; Wang, J.-L.; Lin, W. *J. Am. Chem. Soc.* **2014**, *136*, 273−281.
(32) Ellis, W. C.; McDaniel, N. D.; Bernhard, S.; Collins, T. J. *J. Am. Chem. Soc.* **2010**, *132*, 10990−10991.
(33) Bai, Y.; Sekita, M.; Schmid, M.; Bischof, T.; Steinrück, H.-P.; Gottfried, J. M. *Phys. Chem. Chem. Phys.* **2010**, *12*, 4336−4344.
(34) Bai, Y.; Buchner, F.; Kellner, I.; Schmid, M.; Vollnhals, F.; Steinrück, H.-P.; Marbach, H.; Gottfried, J. M. *New J. Phys.* **2009**, *11*, 125004.
(35) Lukasczyk, T.; Flechtner, K.; Merte, L. R.; Jux, N.; Maier, F.; Gottfried, J. M.; Steinrück, H.-P. *J. Phys. Chem. C* **2007**, *111*, 3090−3098.
(36) Zagal, J. H.; Griveau, S.; Silva, J. F.; Nyokong, T.; Bedioui, F. *Coord. Chem. Rev.* **2010**, *254*, 2755−2791.
(37) Hieringer, W.; Flechtner, K.; Kretschmann, A.; Seufert, K.; Auwärter, W.; Barth, J. V.; Görling, A.; Steinrück, H.-P.; Gottfried, J. M. *J. Am. Chem. Soc.* **2011**, *133*, 6206−6222.

DOI: 10.1021/jacs.5b10484
J. Am. Chem. Soc. 2016, 138, 3623−3626